Journal of the Optical Society of Korea, Vol. 3, No. 1, March 1999, pp. 15-19

Transverse spatial laser beam patterns spontaneously formed in the feedback system with a liquid crystal

Young-Shin Park, Young-Chul Noh, Won-Kyu Lee, Jin-Ho Jeon, Jai-Hyung Lee, and Joon-Sung Chang

Department of Physics, Seoul National University, Seoul 151-742, KOREA

(Received November 17, 1998)

The formation of spontaneous transverse optical patterns was investigated in a single feedback mirror system using nematic liquid crystals as nonlinear optical media. By varying the size of an input beam and the feedback distance, we obtained various interesting transverse optical patterns as well as the hexagonal patterns which are predicted theoretically assuming plane wave input. We can explain theoretically these characteristics of various patterns by introducing a ratio of the beam half width and spatial wavelength of the patterns. We have observed that as this ratio increased, the number of spots constituting the patterns also increased. Finally the patterns evolved into the successive hexagon in the transverse plane.

I. INTRODUCTION

While a laser beam propagates through a nonlinear medium, the beam can be distorted due to self-focusing or self-diffraction, etc. After spontaneous transverse patterns of the laser beam were first predicted theoretically first ten years ago, similar optical patterns have been observed in several experiments [1–3]. In the feedback system consisting of a slice Kerr medium and a single mirror, the transverse hexagonal [4–6] patterns formed spontaneously were predicted theoretically assuming plane input wave. O(2) symmetry breaking of the input beam was studied in the simulation, which assumes Gaussian shape of the laser beam [7]. Also several studies have been carried out in the feedback system using nematic liquid crystal [8–11] as a nonlinear medium.

In the present paper, we constructed the feedback system with a single mirror reflecting the forward beam in order to understand the properties of the transverse patterns. It was shown that, under the cylindrical box approximation of the Gaussian input beam, the properties of the transverse spatial patterns were predicted theoretically by introducing a parameter η, the ratio of a half-width and a spatial wavelength Λ of the transverse patterns. W_0 is defined as the radius where the intensity decreases to $1/e^2$ of its maximum. We can obtain a broad range of η by varying the feedback distance and controlling the input beam width. The theoretical description of the dihedral patterns [8] in Bessel function representations was analyzed further and in detail as a function of η about the boundary conditions and the threshold intensity. As η increased, the experimental data were compared with the successive hexagon with six-fold symmetry in the 2-D plane which is predicted assuming an plane input wave.

II. THEORY

The Talbot effect which was first discovered by H. F. Talbot in 1836 can explain simply the formation of the transverse patterns based on the plane input wave. In the case of a feedback system, the light propagating through the nonlinear medium undergoes a small phase modulation due to the nonuniformity or fluctuation of the medium. The phase-modulated wave then propagates toward the mirror and is reflected back to the medium to become an amplitude-modulated wave. The feedback loop is closed when the reentering beam changes into a phase-modulated beam propagating through the medium again. Based on the Talbot effect, according to the feedback distance, the transverse patterns are built up with the spatial frequency as follows;

$$q_{Talbot}^2 = \frac{\pi^2}{\lambda d}(1+4n) \qquad n = 0, 1, 2, \ldots \tag{1}$$

where d is the feedback distance and λ is the wavelength of the beam. In the case of a liquid crystal it is well known that $n = 0$ [6].

Now let us describe the feedback system in general. From the Maxwell equations, two equations describing the propagation through the liquid crystal cell and in free space can be derived using the slowly varying

envelope approximation. Especially when the beam propagates in the liquid crystal cell we should consider the intensity dependent refractive index which is related as $n(I) = n_0 + n_2 I$. If the electric field of the beam entering the cell is E_F and the electric field of the beam reflected by a mirror is E_B in front of the cell, the two equations for E_F and E_B are [4],

$$\frac{\partial E_F}{\partial z} - i\, n_2\, I\, k_0\, E_F = 0 \tag{2}$$

$$\frac{\partial E_B}{\partial z} - \frac{i}{2k_0}\nabla_\perp^2 E_B = 0 \tag{3}$$

where $k_0 = \frac{2\pi}{\lambda}$ and I is the intensity of the input beam. In Eq.(2) if $n_2 > 0$ it is the case of self-focusing and if $n_2 < 0$, the self-defocusing case. The liquid crystal which is used in the present experiment is known to be self-focusing material ($n_2 > 0$). Eq.(2) describes the propagation through the cell and Eq.(3) describes the propagation in free space.

Another equation describes a nonlinear process generated from the interaction between the laser beam and the medium. In the case of a liquid crystal as a Kerr slice and from the well-known Erickson-Leslice equation [12] which describes the reorientation of the director exposed in the external field, the variation of the transverse refractive index of the liquid crystal at the center of the cell can be derived as follows,

$$\tau_r \frac{\partial \overline{n_0}}{\partial t} - \xi^2\, \nabla_\perp^2 \overline{n_0} + \overline{n_0} = \kappa\, E'^2 \tag{4}$$

where τ_r is the relaxation time and κ represents the amount of the nonlinearity and $\nabla_\perp^2$ is the two dimensional Laplacian perpendicular to the direction of the beam propagation. ξ is called the diffusion length, which is much greater than the wavelength of the laser, so the optical interference at the cell between the forward and backward beam can be neglected. Eq.(2), Eq.(3) and Eq.(4) are general equations describing the feedback system using a liquid crystal as a Kerr slice medium.

In Ref.8 it was reported that, under the cylindrical approximation with input beam of radius W_0, the transverse patterns could be represented as a superposition of the Bessel functions as follows,

$$\overline{n_{0,sp}} = \begin{cases} AJ_m(q\rho)\,\cos m\phi, & 0 \le \rho \le W_0 \\ BK_m(\frac{\rho}{\xi})\,\cos m\phi, & W_0 \le \rho \end{cases} \tag{5}$$

where $\overline{n_{0,sp}}$ is the spatial part of $\overline{n_0}$ and q is the spatial frequency of the patterns and J_m, K_m are the first and second kind of the Bessel function respectively. m is an integer and A, B are constants and can be determined by the boundary conditions.

Here we defined two new parameters η, the spatial frequency times the radius of the input beam which is assumed as a cylindrical box, and α, the inverse of the spatial frequency multiplied by the diffusion length of the liquid crystal as follows,

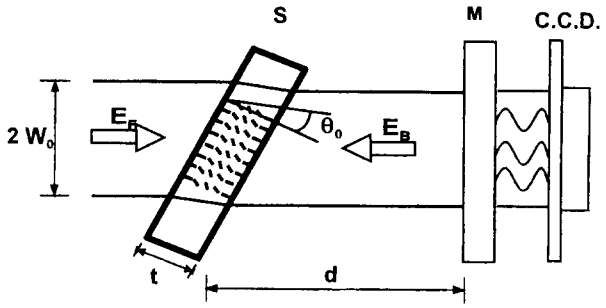

FIG. 1. The feedback system. The forward beam through the sample (S) reenters it after being reflected by a mirror (M). β_0 : tilt angle, d : feedback distance, t : thickness of the sample.

$$\eta = qW_0 = 2\pi\frac{W_0}{\Lambda} \tag{6}$$

$$\alpha = \frac{1}{q\xi} = \frac{1}{2\pi}\frac{\Lambda}{\xi}$$

Using additional boundary conditions, continuities of $\overline{n_{0,sp}}$ and the derivative of $\overline{n_{0,sp}}$ at $\rho = W_0$, we can get the following relationship which includes the new parameters η and α.

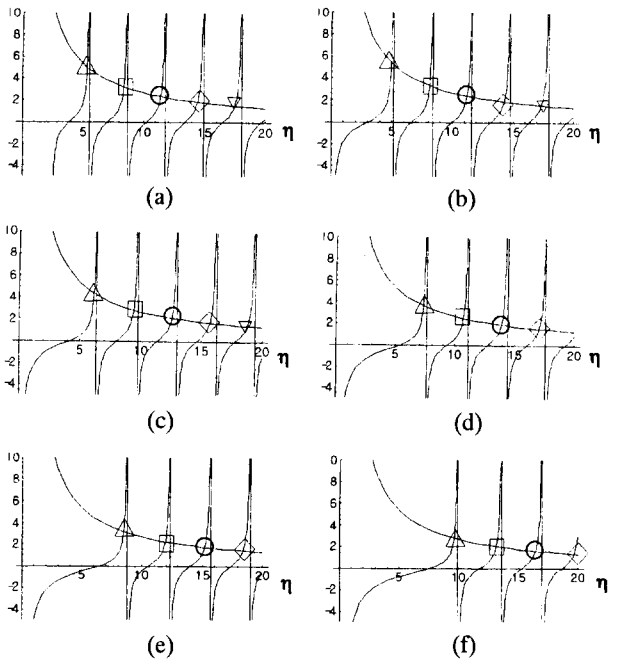

FIG. 2. Graphical solutions according to Eq.(8) for various m. (a) $m = 0$, (b) $m = 2$, (c) $m = 3$, (d) $m = 4$, (e) $m = 5$, (f) $m = 5$. Note that experimental data support that the third group is meaningful.

$$\alpha = -\frac{J_m(\eta)\ [K_{m-1}(\alpha\eta) + K_{m+1}(\alpha\eta)]}{K_m(\alpha\eta)\ [J_{m-1}(\eta) - J_{m+1}(\eta)]} \tag{7}$$

As in Fig.2 for a given m we can obtain graphical solutions by plotting numerically the left and right side of Eq.(7) as a function of η in the case of $W_0 = 1.07\ mm$ and $\xi = 40\ \mu m$. Each group of solutions which are denoted with the same mark increase as mode number m increases, except $m = 0$. In order to determine the meaningful one of the infinite group of solutions, we should consider the threshold intensity curve which is derived from $\overline{n_{0,t}}$, the time part of $\overline{n_0}$. The solution of the time part has a form of $\overline{n_{0,t}} \sim e^{-\frac{t}{\tau}}$ where the constant τ is given as [8],

$$\tau = \frac{\tau_r}{1 + \xi^2 q^2 - \kappa' R E' \sin\frac{d}{k} q^2} \tag{8}$$

where $\kappa' = 2\chi k_0 \frac{d'}{\pi}$ and R is reflectance and E' is a reduced electric field normalized to Fredric transtion field. If $\tau^{-1} > 0$, the solution decays exponentially and the shape of the beam is stable as the time increases. But if $\tau^{-1} < 0$, the solution increases exponentially and the shape becomes unstable. Thus we determined the threshold intensity E'^2_{th} where the formation of the patterns begins. From $\tau^{-1} = 0$, we obtain,

$$E'^2_{th} = \frac{1}{\kappa' R} \frac{1 + (\frac{\xi}{W_0})^2 \eta^2}{\sin[\frac{d\eta^2}{k_0 W_0^2}]} \tag{9}$$

¿From Eq.(9) we can calculate η values in terms of the feedback distance d or half-width W_0 by minimizing the threshold intensity for a fixed W_0 and d. After several fixed W_0 are used, we can obtain a graph like Fig.6 of η as a function of feedback distance d by minimizing the threshold intensity. Especially for $W_0 = 1.07\ mm$, when the curve (b) in Fig.6 was compared with the graphical solution in Fig.2, we can tell that the third group solution has a clear meaning. We have to consider the graphical solutions for each mode as a representative value, so we expect that experimental values of η were distributed about this representative value. The marks in Fig.6 are experimental data and will be discussed in a later section.

We deduce that the dimensionless parameter η is closely related to the spatial pattern and as η increases, both by magnifying the input beam half width and by shortening the feedback distance, the mode m of transverse patterns also increases in order. Therefore we can obtain various dihedral patterns by controlling η.

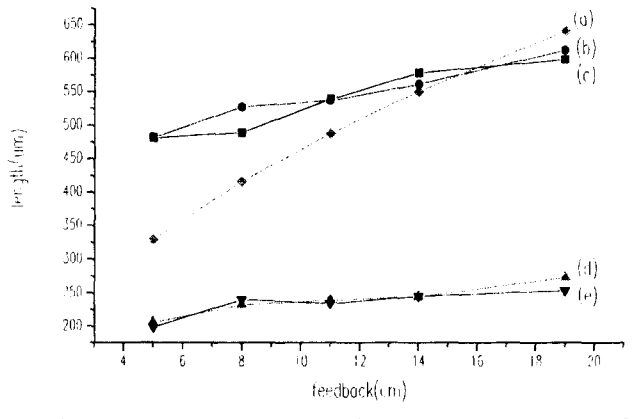

FIG. 3. Spatial wavelength (a) based on the Talbot effect in Eq.(1) with $n = 0$ (b) for $W_0 = 1.07\ mm$ (c) for $W_0 = 1.28\ mm$ in the experiment as a function of feedback distance d. (d) & (e) show that half width of the spots increases for $W_0 = 1.07\ mm$, $W_0 = 1.28\ mm$ respectively.

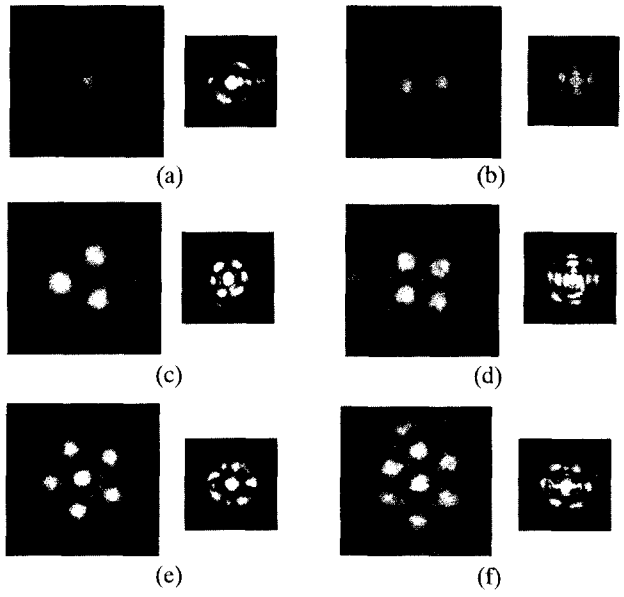

FIG. 4. Near field and far field for various dihedral patterns. (a) ring $[J_0(\rho)]$: $d = 8.3\ cm$, $W_0 = 1.07\ mm$, $I_{input} = 10.0\ W/cm^2$, $\eta = 14.7$ (b) two spots $[J_2(\rho)\mathrm{Cos}(2\phi)]$: $d = 11.0\ cm$, $W_0 = 0.83\ mm$, $I_{input} = 23.1\ W/cm^2$, $\eta = 9.5$ (c) triangular $[J_3(\rho)\mathrm{Cos}(3\phi)]$: $d = 18.0\ cm$, $W_0 = 1.07\ mm$, $I_{input} = 24.2\ W/cm^2$, $\eta = 11.0$ (d) tetragonal $[J_4(\rho)\mathrm{Cos}(4\phi)]$: $d = 12.5\ cm$, $W_0 = 1.07\ mm$, $I_{input} = 28.2\ W/cm^2$, $\eta = 12.4$ (e) pentagonal $[J_0(\rho) + J_5(\rho)\mathrm{Cos}(5\phi)]$: $d = 9.5\ cm$, $W_0 = 1.07\ mm$, $I_{input} = 15.7\ W/cm^2$, $\eta = 15.3$ (f) hexagonal $[J_0(\rho) + J_6(\rho)\mathrm{Cos}(6\phi)]$: $d = 16.5\ cm$, $W_0 = 1.61\ mm$, $I_{input} = 16.7\ W/cm^2$, $\eta = 21.0$.

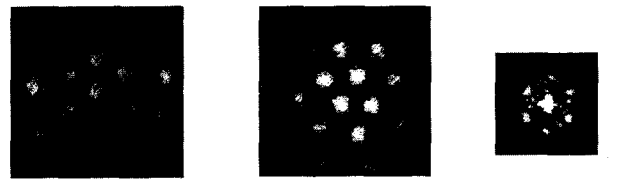

FIG. 5. Hexagonal pattern in 2 - Dimensions. (a) $d = 8.0\ cm$, $W_0 = 1.45\ mm$, $I_{input} = 20.8\ W/cm^2$, $\eta = 21.5$ (b) $d = 8.0\ cm$, $W_0 = 1.61\ mm$, $I_{input} = 15.2\ W/cm^2$, $\eta = 25.1$ (c) far field corresponding to (b).

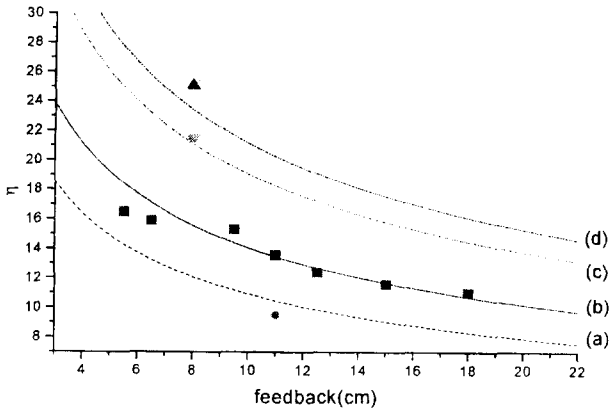

FIG. 6. Relation between η and d derived from threshold curve. (a) $W_0 = 0.83\ mm$, (b) $W_0 = 1.07\ mm$, (c) $W_0 = 1.45\ mm$, (d) $W_0 = 1.61\ mm$. Dots represent experimental data. Circle : $W_0 = 0.83\ mm$, Square : $W_0 = 1.07\ mm$, down triangle : $W_0 = 1.45\ mm$, up triangle : $W_0 = 1.61\ mm$.

III. EXPERIMENT AND RESULT

In the experiment the nematic liquid crystal used as a nonlinear medium was homeotropically arranged between two glass plates coated with HTAB (cetyltrimetyl-ammonium bromide) solution. A linearly polarized Ar-ion laser with wavelength 514.5 nm and Gaussian transverse intensity distribution has been used. We found that the radius at which the intensity of the laser falls to $1/e^2$ from its maximum is 1.07 mm. As in Fig.1 we tilted the sample to make the angle $\theta_0 = 45^o$ between the direction of the propagation of the beam and the normal plane vector of the glass plate. The reflectance of the feedback mirror was found to be $R = 0.87$ and the signals leaking through the feedback mirror were captured by a CCD camera just behind the mirror. The cell thickness was about 120 μm and so the diffusion length ξ is much greater than the wavelength of the beam. Putting a lens with focal length $f = 20\ cm$ just behind the feedback mirror, the far field images corresponding to each near field were obtained at the focal plane. For a broad range of η, we moved the feedback mirror from $d = 5\ cm$ to $d = 20\ cm$ and used several convex lenses which have several different focal lengths. The original widths was $W_0 = 1.07\ mm$ and the modified half width were measured at $W_0 = 0.83\ mm, 1.28\ mm, 1.45\ mm, 1.61\ mm$. However, the modification does not affect the Gaussian shape during the experiment.

In Fig.3 the spatial wavelength Λ of the patterns as a function of feedback distance d were compared with theoretical predictions based on the Talbot effect denoted as (a). As the feedback distance increases, Λ also increases gradually but the change of measured spatial wavelength is slower than for the Talbot effect. Also it is considered that the difference which is large for short feedback range comes from the Gaussian shape of input beam. Fig.3 shows that Λ does not depend on the size of the input beam for two different half widths $W_0 = 1.07\ mm$ and $W_0 = 1.28\ mm$. Therefore this indicates that if we enlarge the size of the input beam, we may expect additional spots in the outer region, maintaining spatial wavelength for a given d. Since the spatial wavelength increases with feedback distance regardless of input beam size, the dimensionless parameter η in Eq.(7) is expected to increase as d decreases for a given input beam. We also found that the intensity distribution of spots constituting the transverse patterns has a Gaussian shape the same as input beam. The measured half width of the spots also increases very slowly with feedback distance but is independent of d, like Λ.

We have obtained various clear dihedral patterns from two spots to hexagon and measured spatial wavelength and input beam half width about each transverse patterns in Fig.4. The values of η were found to be 14.7 for ring, 9.5 for two spots, 11.0 for triangle, 12.4 for rhombus, 15.3 for pentagon and 21.0 for hexagon respectively. The dihedral patterns with higher mode m ($m \leq 6$) have also higher values of η as expected in the theory. The value η of the hexagon was measured as twice as that of two spots. Because the spacing of η between neighboring modes was large for higher m, the region of η forming a pattern with mode m is expected to widen. When these measured η's were compared with graphical solutions in Fig.2, we found that the nearest group is the third one for $W_0 = 1.07\ mm$.

When we increased η further above the value of hexagon formation, the dihedral patterns evolved into successive hexagonal patterns in the transverse plane as in Fig.5. The measured values of η in Fig.5 are 21.5 for (a) and 25.1 for (b) and these values are greater than for other dihedral patterns in Fig.3. We plotted η as a function of d by minimizing the threshold intensity for several values of W_0 in Fig.6 and also denoted experimental data, which agreed well with the theoretical curve.

On the other hand, we investigated several dihedral patterns to compare with theoretical Bessel representation according to Eq.(5) and we also observed far field images as well as near field ones as shown in Fig.4. We did not observe the precise tetragonal pattern in Bessel representation and the shape of the four spots constituting the observed pattern is similar to a rhombus not a square with a central spot. Other dihedral patterns agreed well with Bessel representation. While theoretically we may expect the above hexagon patterns, we did not observe those patterns, which is considered to be the limit of the cylindrical approximation of Gaussian beam. In Ref. [7] it was reported that the far field has six-fold symmetry regardless of the near field pat-

terns in a simulation with the Gaussian shape of the input beam. But on the contrary in our experiment the far field images, which are Fourier transforms of near field images, have the symmetry of each near field pattern. Except for triangular and hexagonal patterns other dihedral patterns do not have six-fold symmetry. The far field image of the pentagon has five additional dimmer spots between neighboring bright spots, which are built up from the phase difference between wave vectors representing five spots in near field patterns. And the far field image corresponding to tetragonal has also four-fold symmetry.

IV. CONCLUSION

We investigated the spontaneous transverse patterns in the feedback system using a nematic liquid crystal as a nonlinear medium. Under the cylindrical approximation of the input beam intensity we can explain the properties of the various transverse patterns by introducing a parameter η, a ratio between input beam half width and spatial wavelength of the patterns. It was found that as we increased η the spontaneous transverse patterns changed in turn from two spots to hexagon and finally transferred into successive hexagons in the 2-D plane. From this phenomenon we deduced that for the dihedral patterns which include from two spots to hexagon, the Gaussian shape of the input beam with limited size strongly affected the structure of the patterns. For large η, we can obtain the successive hexagonal patterns in 2-D because of the approximation of the laser beam to plane wave in the region around center where the variation of intensity is very small. On the other hand, the various transverse patterns are understood as a portion of successively and uniformly distributed hexagonal pattern in the transverse plane. The larger the region above the threshold intensity for forming spontaneous patterns gets, the more spots appear constituting the pattern making a proper symmetry.

However, when the laser intensity increased further, the concentric multirings which were observed in the case of a single pass through liquid crystal above the Fredric intensity formed in the experiment. The multirings include traces of the dihedral patterns. The number of rings increased to a maximum of about fifteen as laser intensity increased.

REFERENCES

[1] G. Grynberg et al., Opt. Commun. **67**, 363 (1988).
[2] M. Kreuzer, W. Balzer, and T. Tschudi, Appl. Opt. **29**, 579 (1990).
[3] N. B. Abraham and W. J. Firth, J. Opt. Soc. Am B **7**, 951 (1990).
[4] W. J. Firth, J. Mon. Opt. **37**, 151 (1990).
[5] G. D'Alessandro and W. J. Firth, Phys. Rev. Lett. **66**, 2597 (1991).
[6] G. D'Alessandro and W. J. Firth, Phys. Rev. A **46**, 537 (1992).
[7] F. Papoff, G. D'Alessandro, G.-L. Oppo, and W. J. Firth, Phys. Rev. A **48**, 634 (1993).
[8] R. Macdonald and H. Danlewski, Opt. Commun. **113**, 111 (1994).
[9] R. Macdonald and H. J. Eichler, Opt. Commun. **89**, 289 (1992).
[10] M. Tamburrini, M. Bonavita, S. Wabnitz, and E. Santamato, Opt. Lett. **18**, 855 (1993).
[11] E. Ciaramella, M. Tamburrini, and E.Santamato, Phys. Rev. A **50**, R10 (1994).
[12] I.-C. Khoo and S.-T. Wu, *Optics and Nonlinear Optics of Liquid Crystal*, (World Scientific, Singapore, 1993) Ch 2.